First-principles calculation of the electronic structure for a bielectrode junction system under strong field and current

Kenji Hirose* and Masaru Tsukada
Department of Physics, Faculty of Science, University of Tokyo, Hongo 7-3-1, Bunkyo-ku, Tokyo 113, Japan
(Received 17 October 1994)

We present a method for the first-principles calculation of the electronic states under strong field and current, which is effective for the bielectrode system with atomic structures around the surface regions. A microscopic electron distribution is calculated self-consistently together with the field and current distributions. In our method the scattering waves are calculated by the step-by-step recursion-matrix method and two different Fermi levels are assigned to each jellim electrode in accord with a given applied bias voltage. The method is applied to the Na/vacuum/Na junction system with a tip structure to mimic the scanning tunneling microscopy (STM). The tip-surface chemical interaction induced by the electric field is clarified and shown to provide a clue for the extreme site specificity of atom extraction by STM.

I. INTRODUCTION

A number of interesting phenomena, such as field emission, field desorption, field evaporation, and surface electromigration, take place on a solid surface in a strong electric field and current.[1–4] Such phenomena have been important not only for basic science but also for the development of technological applications such as field-emission microscopy (FEM), field-ion microscopy (FIM), and scanning tunneling microscopy (STM).[5] Recently much attention has been devoted to the nanometer-scale fabrication technology by use of STM, which has made it possible to manipulate a single atom on a surface. A number of exciting experiments have been performed, and significant proposals have been raised. Examples of such studies involve a transfer of an adsorbed Xe atom between the Ni surface and the W tip called the atom switch,[6] deposition of molecules and mounts of atoms on a surface,[7] site-specific extraction of Si atoms from a surface,[8–10] and others. Such nanometer-scale fabrication technologies are now called atom manipulation, and are expected to bring revolutionary technological developments toward creating atom-scale electronic devices.

These experiments have been performed within a few Å separation between a tip and a surface under an applied bias voltage of several volts. The distance is short and the applied bias voltage high compared with those in observing surface atoms. In such conditions, due to the close proximity between the tip and the surface, a number of effects such as the tip-surface chemical interaction as well as applied strong electric field ($\sim$V/Å) and current ($\sim$100 nA), give rise to atomic processes on the surface. A perturbative approach for electron tunneling, which has been used to analyze the images of STM under electric field ($\sim$0.1 V/Å) and current ($\sim$1 nA),[11,12] is no longer applicable since the overlap of the wave functions of the tip and surface becomes so significant that they cannot be treated separately. In order to obtain a theoretical clue to solving these phenomena, it is necessary to treat the nanometer-scale junction which includes both the tip and surface as a whole system with their atomic structures, and find its electronic structure under strong electric field and current based on a reliable first-principles calculation.

The purpose of the present paper is to develop a microscopic theory of a nanometer-scale junction system under strong electric field and current based on a nonperturbative, self-consistent calculation, and to present its applicability for a Na/vacuum/Na junction including the atomic structures in the surface regions, and to treat the problems of atom extraction by STM. For that purpose, the first problem is that the system inherently loses periodic structure in the direction in which the electric current is flowing. Therefore conventional repeated slab models or cluster models break down. Instead of solving the eigenstates of these models, we have used scattering waves to represent the electronic state of this system. This enables us to assign different Fermi levels E_F^L and E_F^R to the transmitted waves in each electrode, and to obtain the self-consistent electronic structure by treating the Fermi-level difference, i.e., the applied bias voltage as an external parameter. The next problem is that both the microscopic electric field and the electronic structure must be determined in a self-consistent manner to treat a screening effect properly on an atomic scale. An accurate description of the tails of the wave functions in the vacuum region is essential for that. Several WKB methods for the three-dimensional systems proposed so far[13,14] are rather poor for quantitative arguments of realistic systems. The standard linear-combination-of-atomic-orbitals (LCAO) method fails to reproduce accurate tails of the wave functions for relatively wide vacuum gaps. The plane-wave expansion requires us to take a large number of plane waves to describe the tails of the wave functions. Instead, we have solved the coupled-channel equation numerically in the direction normal to the surface. Since a wave-function-matching technique by means of a transfer matrix[15] is known to be numerically unstable due to the appearance of growing evanescent waves, we have developed a recursion-matrix method for

this calculation, in which the matrix ratio between two successive mesh points is treated numerically step by step in a recursive way. Then the effective potential is constructed with the Hartree potential, ion-core pseudopotential, and exchange-correlation potential, where we have used the local-density approximation (LDA), and the calculation is repeated until the convergence of the effective potential is achieved. In such a way, the electron-density profile, effective potential, and electric current are calculated self-consistently without any difficulties of numerical divergence of wave functions.

Historically, earlier calculations for the bimetallic junction were performed by Benett and Duke[16] and Ferrante and Smith[17] with use of jellium surfaces. The development of STM has raised a renewed interest in the electron tunneling through a metal/vacuum/metal junction system. Orosz and Balázs[18] and McCann and Brown[19] performed a self-consistent calculation of the potential barrier through a jellium junction by imposing an applied bias voltage based on the LDA. Recently Lang has made several self-consistent calculations involving an adsorbed atom between jellium electrodes subject to a large voltage difference,[20] and investigated the atom transfer between electrodes.[21] Ciraci, Baratoff, and Batra performed computations for the metallic slabs with atomic structures, though the effect of the applied bias voltage was not taken into account.[22] The present method enables us to include atomic structures in the surface regions as well as the effect of the electric field and current, and thus affords a further step for the understanding of the microscopic processes of atom extraction by the tip.[23] For other applications, this method is applicable to various fields such as the microscopic theory of field emission and field desorption and evaporation, standing-wave excitations, adsorbate-covered surfaces, microcontacts, and ballistic electron emission microscope (BEEM).

The paper is organized as follows: The method of the present calculation is explained in detail in Sec. II. The results of application to the planar Na junction are described in Sec. III. The method is further applied to the problems of STM around the contact region in Sec. IV in which the tip-surface interaction as well as field and current plays an important role. In Sec. V we incorporate the atom extraction by the tip toward a full understanding of the microscopic processes. The calculated results of electron-density profiles and adiabatic potential curves are presented. Section VI is devoted to concluding remarks.

II. METHOD OF CALCULATION

A. Recursion-transfer-matrix method

The model we consider is a bielectrode system in which several atomic layers are attached to the left and right semi-infinite jellium electrodes with Fermi levels of E_F^L and E_F^R (see Fig. 1). The atomic layers have a supercell structure to minimic a real tip shape and a surface. The parameters included are the applied bias voltage V and the radius r_s, which is related to the electron density of the jellium ρ_+ through $1/\rho_+=\frac{4}{3}\pi r_s^4$. Throughout this paper we use the atomic units $|e|=\hbar=m=1$, in which the unit length is a_B (1 Å$=0.529a_B$).

Taking the z axis normal to the surface, and assuming two-dimensional (2D) translational symmetry parallel to the surface, we can express the wave function by a Laue representation as

$$\Psi_j(\mathbf{r})=e^{i\mathbf{k}_\parallel\cdot\mathbf{r}_\parallel}\sum_i \psi_{ij}(z)e^{i\mathbf{G}_\parallel^i\cdot\mathbf{r}_\parallel}\ , \tag{1}$$

where j is the incident channel number and $\{\mathbf{G}_\parallel^i\}$ is a set of 2D reciprocal-lattice vectors. The unknown coefficient functions $\psi_{ij}(z)(i,j=1,2,\ldots,N)$ form the matrix $U(z)$, which obeys the following equation:

$$\frac{1}{2}\frac{d^2}{dz^2}U(z)=V(z,E)U(z)\ , \tag{2}$$

with the matrix $V(z,E)$:

$$V(z,E)=\begin{bmatrix} V_0(z)+\frac{1}{2}|\mathbf{k}_\parallel+\mathbf{G}_\parallel^0|^2-E & V_1(z) & \cdots \\ V_{-1}(z) & V_0(z)+\frac{1}{2}|\mathbf{k}_\parallel+\mathbf{G}_\parallel^1|^2-E & \cdots \\ \vdots & \vdots & \ddots \end{bmatrix}. \tag{3}$$

Here $V_{i-j}(z)$ is the Fourier coefficient of the effective potential $V_{\text{eff}}(\mathbf{r})$ in the lateral direction $\mathbf{r}_\parallel$,

$$V_{i-j}(z)=\frac{1}{S}\int V_{\text{eff}}(\mathbf{r})e^{-i(\mathbf{G}_\parallel^i-\mathbf{G}_\parallel^j)\cdot\mathbf{r}_\parallel}d\mathbf{r}_\parallel\ , \tag{4}$$

where S is the area of the unit cell.

In the present system, the wave functions for an energy E are classified into two categories of linearly independent solutions: $\Psi_j^L(\mathbf{r})$, whose incident waves come from the left electrode; and $\Psi_j^R(\mathbf{r})$ from the right electrode. These states form the matrix $U^L(z)$ and $U^R(z)$. Due to the screening effect of the metallic jellium, the effective potential tends to take constant values deep in the jellium electrodes. Thus in the case of $\Psi_j^L(\mathbf{r})$ it is composed of an incident wave (channel number j) and the reflected waves deep in the left electrode,

$$\Psi_j^L(\mathbf{r})=e^{ik_z^j z}e^{i(\mathbf{k}_\parallel+\mathbf{G}_\parallel^j)\cdot\mathbf{r}_\parallel}+\sum_i r_{ij}\begin{Bmatrix} e^{-ik_z^i z} \\ e^{\kappa_z^i z}\end{Bmatrix}e^{i(k_\parallel+\mathbf{G}_\parallel^i)\cdot\mathbf{r}_\parallel}\ , \tag{5}$$

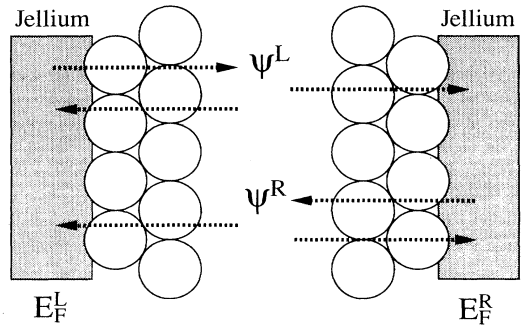

FIG. 1. Schematic representation of the present bielectrode junction system. The jellium model is used for each electrode and several layers of atoms are attached to the left and right jellium electrodes with Fermi levels of E_F^L and E_F^R.

and it is composed of the transmitted waves deep in the right electrode:

$$\Psi_j^L(\mathbf{r})=\sum_i t_{ij}\begin{Bmatrix} e^{ik_z^i z} \\ e^{-\kappa_z^i z}\end{Bmatrix} e^{i(\mathbf{k}_\parallel+\mathbf{G}_\parallel^i)\cdot\mathbf{r}_\parallel}\ , \tag{6}$$

where r_{ij} and t_{ij} are the elements of an unknown reflected and transmitted matrix, respectively. { } represents taking either form corresponding to the wave vector in the z direction. A similar expression is also obtained for $\Psi_j^R(\mathbf{r})$.

In order to solve the coupled differential equation, the recursion-matrix method has been used. First the z axis is divided into fine meshes $\{z_p;p=0,\ldots,l+1\}$ with the mesh width $h=z_{p+1}-z_p$, where the terminated points z_0 and z_{l+1} are taken deep in each jellium electrode. Then the matrix equation (2) is transformed into the difference-matrix equation[24]

$$a(z_p)U^{L(R)}(z_{p+1})-b(z_p)U^{L(R)}(z_p) +c(z_p)U^{L(R)}(z_{p-1})=0\ , \tag{7}$$

where

$$\begin{aligned} a(z_p)&=I-\tfrac{1}{6}h^2V(z_{p+1},E)\ ,\\ b(z_p)&=2I+\tfrac{5}{3}h^2V(z_p,E)\ ,\\ c(z_p)&=I-\tfrac{1}{6}h^2V(z_{p-1},E)\ , \end{aligned} \tag{8}$$

with the unit matrix I and $V(z,E)$.

The ratio matrix on the neighboring mesh points

$$S(z_p)=U^{L(R)}(z_{p+1})U^{L(R)}(z_p)^{-1} \tag{9}$$

satisfies a recursion-matrix equation

$$S(z_{p-1})=[b(z_p)-a(z_p)S(z_p)]^{-1}c(z_p)\ . \tag{10}$$

Note that matrices $a(z_p)$, $b(z_p)$, and $c(z_p)$ are all determined once the matrix $V(z_p,E)$ is given.

Deep in the jellium electrodes ($z\le z_0, z\ge z_{l+1}$), $V_{\text{eff}}(\mathbf{r})$ takes constant values V^L or V^R, and thus the matrix $V(z,E)$ becomes diagonal. Note that the Friedel oscillations are omitted outside the terminated points z_0 and z_{l+1} in this formalism. This effect on electronic structures around the surface regions becomes small if z_0 and z_{l+1} are taken deep in the jellium electrodes. The difference equations in these regions are decoupled for each $\psi_{ij}(z)$ component as

$$[1-\tfrac{1}{6}\beta^{L(R)}]\psi_{ij}(z_{p+1})-[2+\tfrac{5}{3}\beta^{L(R)}]\psi_{ij}(z_p) +[1-\tfrac{1}{6}\beta^{L(R)}]\psi_{ij}(z_{p-1})=0\ , \tag{11}$$

where

$$\beta^{L(R)}=h^2[V^{L(R)}+\tfrac{1}{2}|\mathbf{k}_\parallel+\mathbf{G}_\parallel^i|^2-E]\ . \tag{12}$$

Combining all incident channel states, we obtain the asymptotic forms of the wave functions in the regions ($z\le z_0, z\ge z_{l+1}$):

$$U^L(z_p)=\begin{cases}[K_{(+)}^L]^pA+[K_{(-)}^L]^pR & \text{for } z_p\le z_0\\ [K_{(+)}^R]^pT & \text{for } z_p\ge z_{l+1}\end{cases} \tag{13}$$

and

$$U^R(z_p)=\begin{cases}[K_{(-)}^L]^pT' & \text{for } z_p\le z_0\ ,\\ [K_{(-)}^R]^pA+[K_{(+)}^R]^pR' & \text{for } z_p\ge z_{l+1}\ ,\end{cases} \tag{14}$$

where Λ denotes a diagonal phase matrix, which does not affect the electron density or the current density, and R, R', T, and T', respectively, denote unknown matrices.

$K_{(\pm)}^{L(R)}$ in (13) and (14) is defined as

$$K_{(\pm)}^{L(R)}=\begin{bmatrix} g_{(\pm)}^{L(R)}(\mathbf{G}_\parallel^0) & & & \\ 0 & g_{(\pm)}^{L(R)}(\mathbf{G}_\parallel^1) & 0 & \cdots\\ & \vdots & g_{(\pm)}^{L(R)}(\mathbf{G}_\parallel^2) & \ddots\end{bmatrix}\ , \tag{15}$$

where

$$g_{(\pm)}^{L(R)}(\mathbf{G}_\parallel^i)=\frac{1+\frac{5}{6}\beta^{L(R)}}{1-\frac{1}{6}\beta^{L(R)}}\pm i\left[1-\left[\frac{1+\frac{5}{6}\beta^{L(R)}}{1-\frac{1}{6}\beta^{L(R)}}\right]^2\right]^{1/2} \quad \text{for } E-\tfrac{1}{2}|\mathbf{k}_\parallel+\mathbf{G}_\parallel^i|^2>V^{L(R)}\ , \tag{16}$$

$$g_{(\pm)}^{L(R)}(\mathbf{G}_\parallel^i)=\frac{1+\frac{5}{6}\beta^{L(R)}}{1-\frac{1}{6}\beta^{L(R)}}\mp\left[\left[\frac{1+\frac{5}{6}\beta^{L(R)}}{1-\frac{1}{6}\beta^{L(R)}}\right]^2-1\right]^{1/2} \quad \text{for } E-\tfrac{1}{2}|\mathbf{k}_\parallel+\mathbf{G}_\parallel^i|^2<V^{L(R)}\ . \tag{17}$$

Note the relation between $K^{L(R)}_{(\pm)}$:

$$K^{L(R)}_{(+)}K^{L(R)}_{(-)}=I \ . \tag{18}$$

In the region $z_0<z_p<z_{l+1}$, where the Fourier components $V_{i-j}(z)$ remain finite and thus the difference-matrix equations are not decoupled, the recursion-matrix equation is used for obtaining $U^{L(R)}(z_p)$. Starting the calculation with the matrix $S(z_{l+1})=K^R_{(+)}$, we obtain $S(z_p)$ at an arbitrary point $z_0<z_p<z_{l+1}$. Then by using the relation

$$U^L(z_0)=S(z_{-1})[K^L_{(+)}S(z_{-1})-I]^{-1}[K^L_{(+)}-K^L_{(-)}]\Lambda \ , \tag{19}$$

$U^L(z_p)$ are obtained for each mesh point. The calculation for $U^R(z_p)$ is performed in the same way by changing the index $p\rightarrow l+1-p$.

In the above procedure, the ratios of the wave functions $S(z_p)$ at the neighboring points are first determined by using the boundary conditions in the jellium electrodes instead of treating the wave functions directly. This means that we effectively treat only a derivative at the point p. On the condition that the amplitude of the incident wave is unity, the normalized wave function is obtained. In this calculation the appearance of the growing evanescent waves is avoided in both electrodes, and we have found that the inverse of the matrix $K^L_{(+)}S(z_{-1})-I$ is not singular. This enables us to perform a stable numerical calculation and the wave functions obtained are sufficiently precise. We have checked by investigating the current flux at the terminating points z_0 and z_{l+1} that the truncation error due to the discretization is reduced significantly as the mesh size h becomes small. This is an important merit of this calculation method. The only assumption is that at the boundaries z_0 and z_{l+1} the effective potential is smoothly switched to constant values V^L and V^R.

B. Calculation of potential and current

Here consider the solution of the Poisson equation:

$$\nabla^2 V_H(\mathbf{r})=-4\pi[\rho(\mathbf{r})-\rho_+(\mathbf{r})] \ , \tag{20}$$

where the electron density is constructed by summing the square of the wave functions over the occupied states,

$$\rho(\mathbf{r})=\frac{2}{(2\pi)^3}\sum_{L,R}\sum_j\int_0^{k_f}dk_z^j\int d\mathbf{k}_\parallel|\Psi_j^{L,R}(\mathbf{r})|^2 \ . \tag{21}$$

For the present system, the Poisson equation is rewritten as

$$\left[\frac{d^2}{dz^2}-|\mathbf{G}^i_\parallel|^2\right]V_H(\mathbf{G}^i_\parallel,z)=-4\pi[\rho(\mathbf{G}^i_\parallel,z)-\rho_+(z)\delta_{i,0}] \ , \tag{22}$$

where $\rho_+(\mathbf{r})$ is the positive charge density of the jellium electrodes, and $V_H(\mathbf{G}^i_\parallel,z)$, and $\rho(\mathbf{G}^i_\parallel,z)$ are the Fourier components of $V_H(\mathbf{r})$ and $\rho(\mathbf{r})$.

The solution for $\mathbf{G}^i_\parallel\neq 0$ becomes

$$V_H(\mathbf{G}^i_\parallel,z)=\frac{2\pi}{|\mathbf{G}^i_\parallel|}\int_{z_0}^{z_{l+1}}dz'\rho(G^i_\parallel,z')\frac{e^{-|\mathbf{G}^i_\parallel||z-z'|}+e^{-|\mathbf{G}^i_\parallel|[2(z_{l+1}-z_0)-|z-z'|]}-e^{-|\mathbf{G}^i_\parallel|(2z_{l+1}-z-z')}-e^{-|\mathbf{G}^i_\parallel|(z+z'-2z_0)}}{1-e^{-2|\mathbf{G}^i_\parallel|(z_{l+1}-z_0)}} \tag{23}$$

and the solution for $\mathbf{G}^0_\parallel(=0)$ with the boundary conditions at $z=z_0$ and z_{l+1} satisfies the following self-consistent equation:

$$\begin{aligned}V_H(\mathbf{G}^0_\parallel,z)=\Bigg[&\int_{z_0}^{z_{l+1}}\left\{\frac{2\pi}{K}[\rho(\mathbf{G}^0_\parallel,z')-\rho_+(z')]+\frac{K}{2}V_H(\mathbf{G}^0_\parallel,z')\right\}\\&\times(e^{-K|z-z'|}+e^{-K[2(z_{l+1}-z_0)-|z-z'|]}-e^{-K(2z_{l+1}-z-z')}-e^{-K(z+z'-2z_0)})dz'\\&+V_H(\mathbf{G}^0_\parallel,z_0)(e^{-K(z-z_0)}-e^{-K(2z_{l+1}-z_0-z)})\\&+V_H(\mathbf{G}^0_\parallel,z_{l+1})(e^{-K(z_{l+1}-z)}-e^{-K(z-2z_0+z_{l+1})})\Bigg]\Big/(1-e^{-2K(z_{l+1}-z_0)}) \ .\end{aligned} \tag{24}$$

Here K is an arbitrary constant. The iteration procedure for this equation is remarkably stable, and several iteration steps are sufficient for a good convergence of $V_H(\mathbf{G}^0_\parallel,z)$.[25]

As for the ion-core potential $v^\mu_{\rm ion}$ for each atom μ, we adopt a local empty-core pseudopotential[26]

$$v^\mu_{\rm ion}(r)=\begin{cases}-\dfrac{Ze^2}{r} & \text{for } r\geq r_c\\ 0 & \text{for } r<r_c \ ,\end{cases} \tag{25}$$

where r_c is a cutoff radius.

The Fourier component of $V_{\rm ion}(\mathbf{r})$ is obtained by a straightforward calculation

$$V_{\rm ion}(\mathbf{G}_{\parallel}^{i},z)=\frac{1}{S}\sum_{\mu}e^{-i\mathbf{G}_{\parallel}^{i}\cdot\tau_{\parallel}^{\mu}}v_{\rm ion}^{\mu}(\mathbf{G}_{\parallel}^{i},z-z_{\mu})\ , \tag{26}$$

where

$$v_{\rm ion}^{\mu}(\mathbf{G}_{\parallel}^{i},z-z_{\mu})=\begin{cases}-2\pi Ze^{2}\dfrac{e^{-|\mathbf{G}_{\parallel}^{i}||z-z_{\mu}|}}{|\mathbf{G}_{\parallel}^{i}|} & \text{for } |z-z_{\mu}|\le r_{c}\\ -2\pi Ze^{2}\left[\dfrac{e^{-|\mathbf{G}_{\parallel}^{i}||z-z_{\mu}|}}{|\mathbf{G}_{\parallel}^{i}|}-\displaystyle\int_{0}^{\sqrt{r_{c}^{2}-|z-z_{\mu}|^{2}}}d|\mathbf{r}_{\parallel}|\frac{|\mathbf{r}_{\parallel}|J_{0}(|\mathbf{G}_{\parallel}^{i}||\mathbf{r}_{\parallel}|)}{\sqrt{|\mathbf{r}_{\parallel}|^{2}+|z-z_{\mu}|^{2}}}\right] & \text{for } |z-z_{\mu}|<r_{c}\ .\end{cases} \tag{27}$$

Here $(\tau_{\parallel}^{\mu},z_{\mu})$ is the position of each atom μ is the 2D supercell.

As for the exchange-correlation potential $V_{\rm xc}(\mathbf{r})$, strictly speaking, we have to use the current-density-functional theory for the system in which the current is flowing.[27] However, if the rotation of the current density is not large, the correction due to the current is small and the local-density approximation (LDA) is still effective.[21] Note that the applied magnetic field is absent here. In the present study, we have used the LDA of the Ceperley-Alder form[28] as parametrized by Perdew and Zunger.[29]

The current density distribution $\mathbf{j}(\mathbf{r})$ is obtained as

$$\mathbf{j}(\mathbf{r})=\frac{2e^{2}}{(2\pi)^{3}}\sum_{j}\int dk_{z}^{j}\int d\mathbf{k}_{\parallel}[f(E)-f(E-eV)]S_{j}(\mathbf{r})\ , \tag{28}$$

where

$$S_{j}(\mathbf{r})=\frac{\hbar}{2mi}[\Psi_{j}^{*}(\mathbf{r})\nabla\Psi_{j}(\mathbf{r})-\Psi_{j}(\mathbf{r})\nabla\Psi_{j}^{*}(\mathbf{r})]\ , \tag{29}$$

and $f(E)$ is the Fermi distribution function. In the case that the left electrode is negatively biased, the wave functions $\Psi_{j}^{L}(\mathbf{r})$, whose energy lies between $E_{F}^{R}\le E^{L}\le E_{F}^{L}$, contribute to the electric current. The electric current through the surface area A ($A\gg$unit cell area) is expressed as

$$\mathbf{J}=\sum_{i,j}\int_{E_{F}^{R}}^{E_{F}^{L}}dE\int\frac{d\mathbf{k}_{\parallel}}{(2\pi)^{2}}\frac{2e^{2}}{h}|T_{i,j}|^{2}A\ , \tag{30}$$

where $T_{i,j}=t_{i,j}\sqrt{k_{z}^{i}/k_{z}^{j}}$ is the transmission matrix. Here the decaying evanescent wave $e^{-\kappa_{z}^{i}z}$ does not contribute to the current density.

It is shown that the matrices T and R, whose components are $T_{i,j}$ and $R_{i,j}$, satisfy the unitarity relation

$$\begin{aligned}&T^{*}T+T^{*}R=I\ ,\\ &T=T^{T}\ ,\\ &R=R^{T}\ ,\end{aligned} \tag{31}$$

where $R_{i,j}=r_{i,j}\sqrt{k_{z}^{i}/k_{z}^{j}}$ is the reflection matrix, T^{T} and R^{T} are the transported matrices, and T^{*} and R^{*} are the complex-conjugate matrices of T and R, respectively.

III. APPLICATION TO SODIUM PLANAR JUNCTION UNDER ELECTRIC FIELD AND CURRENT

In Sec. II, we presented a method for calculating the electronic structure of a junction system, including the atomic structure for an applied finite bias voltage, which enables us to describe a delicate interplay between the electron density and the electric field and current. The method goes far beyond perturbation and provides us with a fundamental theoretical device to treat various electronic and atomic phenomena occurring on the surface under strong electric field and current from a microscopic standpoint.

In order to examine the applicability of our method, we treat the planar Na junction system here, which is well described by a weak pseudopotential. We consider the system in which two layers of Na are attached to the jellium electrodes with $r_{s}=2.0$. The origin of the z coordinate is chosen at the center of the vacuum, and the separation d is defined by the distance between the top-layer atoms of both surfaces. The Na atoms are positioned symmetrically, maintaining the ideal atomic positions of the (001) surfaces. For simplicity, the reconstruction of the surface atoms is not considered. The distance between the edge of the jellium electrode and the nearest Na atoms to the jellium is fixed at $3.0a_{B}$, and the calculation is started at the point of $7.0a_{B}$ deep in the jellium electrode from its edge. The mesh size h is taken as $0.5a_{B}$, and 16 $\mathbf{k}_{\parallel}$ points for 20 k_{z}^{j} points are taken for each calculation of $\Psi_{j}^{L}(\mathbf{r})$ and $\Psi_{j}^{R}(\mathbf{r})$, respectively. The bias voltage is applied with the left electrode negative. Therefore the electron flows from the left to the right, and the electric current is from the right to the left.

Figure 2 shows the calculated results of the effective potential averaged over the parallel plane at the separation of $d=20.0a_{B}$. Negative bias voltages of 0.4 and 2.0 V are applied to the left electrode. The positions of the atomic layers are indicated by arrows below. We have checked that the calculated work function of 2.71 eV, which is obtained at a large separation ($d=50.0a_{B}$) with no applied bias voltage, is close to the experimental value of 2.75 eV due to the inclusion of the effect of the ion cores in the surface regions, and considerably different from the value in the jellium case (3.06 eV for $r_{s}=3.99$).[30] It is seen that the potential barrier height decreases as the

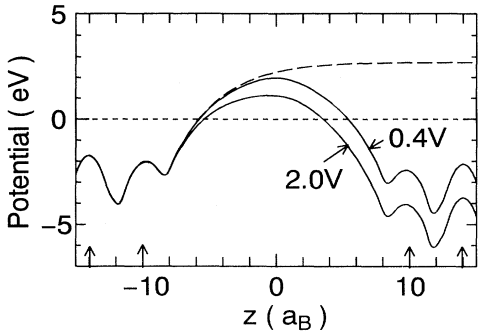

FIG. 2. Effective potential $V_{\text{eff}}(\mathbf{r})$ averaged over the parallel plane. The separation of the two surfaces $d=20.0a_B$. Two cases of bias voltage 0.4 and 2.0 V are shown. The effective potential for the separation $d=50.0a_B$ with zero-bias voltage is shown by the dashed line. The atomic positions are indicated by the arrows below.

applied bias voltage increases. The slope of the potential in the vacuum close to the left (negative) surface goes down, while that close to the right (positive) surface goes up. Therefore as the applied bias voltage increases, the electron density in the negative surface becomes easy to push out in the vacuum region, while the charge density in the positive surface is pushed in. In the present separation $d=20.0a_B$, two surfaces are located so closely that the tails of the electron density in the left and right surfaces overlap significantly with each other in the vacuum region. Therefore the effective potential does not take a straight-line profile even in the middle of the vacuum region.

In Fig. 3, we show the contour plots of the electron-density distribution in the (110) plane. This plane passes the center of atoms for all layers. In these figures the positions of the centers of atoms are indicated by filled dots. In the absence of applied bias voltage, the electron densities are distributed symmetrically in the left and right surfaces. Here the parts in which the electron density takes higher values are located between the Na atoms in the first and second layers. On the other hand, the electron densities at the centers of the Na atoms take low values. This is due to a strong core repulsion of the Na pseudopotential within the range of cutoff radius R_c. Correspondingly the valence electrons are pushed out from the core regions and as a result are located around the middle regions of the lines connecting adjacent Na atoms. With an increase of applied bias voltage, the change of the electron-density distribution is eminent both in the positive and negative surfaces. In the case of an applied bias voltage of 10.0 V, which is actually extremely high, the electron-density profile in front of the surface Na atoms in the negatively biased side (left) is pushed out to the vacuum region and forms large undulating curves there, which suggests that the electric fields concentrate around the atomic sites. On the other hand, the electron-density profile in the positively biased side (right) is pushed inside almost uniformly. This trend is observed more clearly in Fig. 4, which shows the contour plot of the induced electron density $\delta\rho(\mathbf{r})$ on the (110) plane defined as

$$\delta\rho(\mathbf{r})=\rho(\mathbf{r},10.0\text{ V})-\rho(\mathbf{r},0\text{ V})\ . \tag{32}$$

The solid contour indicates that the electron density in that region increases, while the dotted contour indicates the deficiency of the electron density in that region. We note that in the negatively biased side (left) the electron

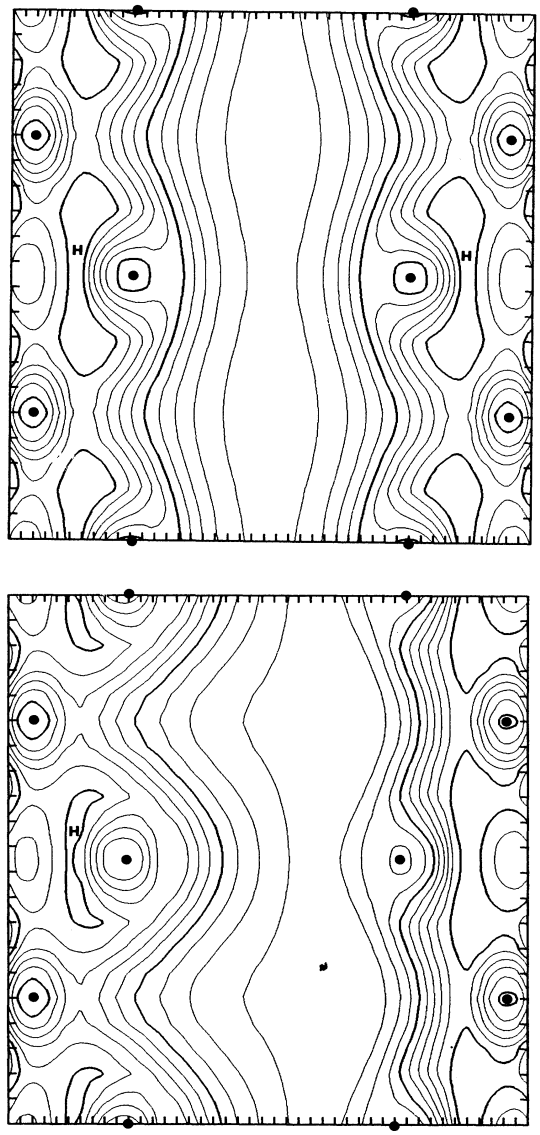

FIG. 3. Electron-density distribution in the (110) plane. The separation of the two surfaces is $d=12.0a_B$. The contour plot is in units of $0.1e/\Omega$, where $\Omega=a^3/2$, $a=8.09a_B$ is the lattice constant. The centers of the atomic positions are indicated by ●. The top view is in the zero-bias case, and the bottom view is in the case of 10.0-V applied bias voltage. The parts in which the electron density takes higher values are indicated by *H*. Note that the electron density takes lower values at the centers of the Na atoms ●.

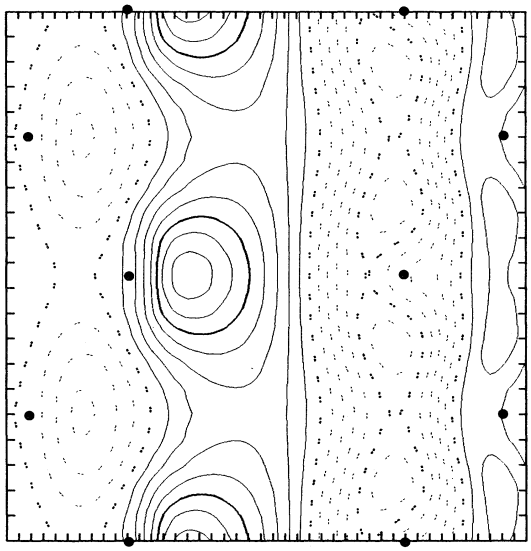

FIG. 4. Induced electron-density distribution $\delta\rho(\mathbf{r})$ due to the 10.0-V applied bias voltage. The separation of the two surfaces is $d=12.0a_B$. The solid line represents the electron excess, and the dotted line represents the electron depletion. The contour plot is in units of $0.05e/\Omega$. The atomic positions are indicated by ●.

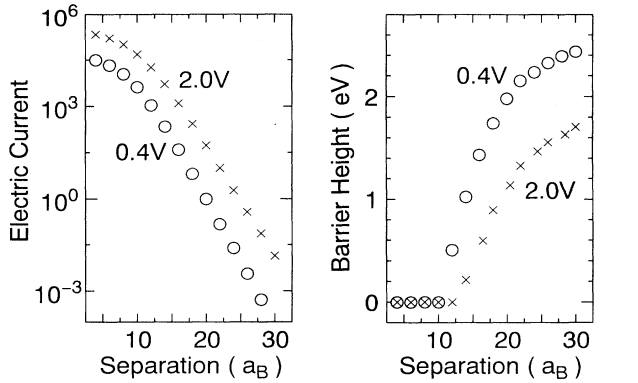

FIG. 5. Electric current (left) and potential barrier height ϕ (right) as functions of the separation d. The electric current is represented in the logarithmic scale, scaled the values in the case of $d=20.0_B$ and 0.4 V applied bias voltage as a unit. Two kinds of applied bias voltages, 0.4 and 2.0 V, are shown.

density increases significantly in front of the atoms in the first atomic layer. In this way, the electron density is drastically changed if a high applied bias voltage is imposed. In the case of a relatively low applied bias voltage, the electron density is not modified so significantly. Such modification of the electron-density distribution on the surface due to the applied bias voltage affords a clue to the mechanism of atom manipulation by STM, as will be seen in Sec. IV.

Next we present calculated results for the electric current and potential barrier height for various separations between the surfaces and for various applied bias voltages. The electric current normalized to the value in the case of $d=20.0a_B$ and 0.4 V is shown in Fig. 5 (left) as a function of the separation d for two kinds of applied bias voltage 0.4 and 2.0 V. It is seen that when the separation d is large, the electric current increases exponentially by about one order of magnitude with the decrease of the separation d by $2.5a_B$. If we assume the constant square-potential barrier with the effective barrier height ϕ_{eff}, the tunneling current density can be written approximately as

$$j \sim V\rho(E_F)e^{-2\kappa d}, \tag{33}$$

for a small applied bias voltage $eV \ll \phi_{\text{eff}}$, where $\kappa=\sqrt{2m\phi_{\text{eff}}/\hbar^2}$. It is interesting to note that it can represent the distance dependence of the calculated electric current in a certain region of d, and that the value of the parameter ϕ_{eff}, giving the best fit to the calculation (~ 3 eV), is close to the experimental work function even at the short separation. Figure 5 (right) shows the calculated potential barrier height ϕ as a function of the separation d. Here ϕ is defined as the maximum value of the laterally average effective potential in the vacuum region. The potential barrier height ϕ approaches the work function if the separation is large enough. It is seen that the potential barrier height ϕ decreases significantly as the separation becomes small. Thus the effective barrier height ϕ_{eff}, which has been often used to estimate the barrier height experimentally, tends to take a larger value compared with the barrier height ϕ.[31]

In the case of a small distance of the separation (shorter than $d=10.0a_B$ in the present Na case), the calculated current is not proportional to the bias voltage, and the increase of the electric current versus the separation is clearly deviated from exponential growth. We can see that at a distance of $10.0a_B$ the potential barrier height disappears and the contact region emerges. Since the potential barrier is missing in this region, the electric current near the Fermi level is dominated by ballistic electrons, and thus the behavior of the electric current is proportional to the incident electron channels. Furthermore the effect of the surface atoms on the shape of the effective potential in the vacuum region cannot be ignored. Therefore the so-called barrier height has no physical meaning in this region. This distance remarkably depends on the applied bias voltage.

According to the experiments performed around the contact region,[8] the electric field and the chemical forces acting on the surface atoms in this region are very strong. Therefore the modification of the electronic structure of the surfaces is significant.[22,32] This effect is important for the atom extraction by using the tip of the scanning tunneling microscope. Thus it is of interest to see the relation between the deformation of the electron-density profile and the onset of the contact region in view of the potential barrier height, since the lowering of the potential barrier height enhances the chemical interaction localized in the narrow channel region. In Fig. 6, we show contour plots of the electron-density profile for different values of the separation. The applied bias voltage is fixed at 2.0 V. In the case of $d=18.0a_B$, the electron density

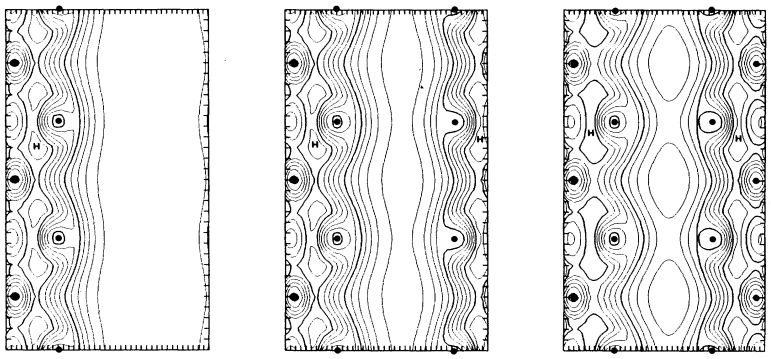

FIG. 6. Electron-density profiles for different values of the separation; $d=18.0a_B$ (left), $12.0a_B$ (center), and $10.0a_B$ (right), respectively. The applied bias voltage is 2.0 V with the left side negative.

decreases smoothly toward the vacuum region. On the other hand, in the case of $d=12.0a_B$, the electron density around the surfaces shows slight undulating curves due to the interaction between them. In the case of $d=10.0a_B$, the electron density of the surfaces is deformed, and shows a concentration in the middle region and forms a bridge structure between the confronting top atoms of the two surfaces. In such a case it is apparent that we cannot treat those surfaces independently. It should be noted that this separation coincides with the distance at which the potential barrier height collapses.

IV. ELECTRONIC STRUCTURE IN THE PRESENCE OF A TIP

To treat a simple model with the tip of STM, we take a large unit cell whose unit length is twice as large as the lattice constant of the bulk in directions parallel to the surface. On the surface, two layers of Na atoms are arranged in the (001) direction. On the tip side, a pyramid structure composed of five Na atoms is assumed. Therefore, in the present model, a total of 13 atoms is included in the unit cell of the superlattice. The reconstruction of these atoms is not taken into consideration. The separation d is defined as the distance between the tip apex atom and the top plane of the surface. The origin of the z coordinate is taken at the middle of the vacuum. We have used the same conditions for the mesh size, the $\mathbf{k}$ points, and the terminating points z_0 and z_{l+1} as those for the Na planar junction system. In this section and those following, V_S means the applied bias voltage of the surface when that of the tip is set zero. For the clear view of the present system, the results are shown with the tip on the top and with the surface on the bottom.

First we present calculated results of the electron-density function for the tip-surface system. The proximity effect of the tip and surface on their electronic structure is of great importance for the purpose of studying atom manipulation by STM. Figure 7 shows the contour maps of the electron-density distribution for tip-surface separations of $d=14.0a_B$ (left) and $10.0a_B$ (right). The applied bias voltage is fixed at $V_S=+2.0$ V for both cases. Note that the parts in which the electron density takes higher values on the tip side are located in the middle region between the tip apex atom and the atoms in the second layer. In the case of $14.0a_B$ separation, the electron-density profiles of the tip and surface show little deformation. This indicates that the effect of the tip on the surface is not so large in this case. We have confirmed that the electron-density profiles are almost unchanged for larger tip-surface separations. In the case of $10.0a_B$ separation, however, the electron-density distributions for both the tip and surface are deformed significantly. Due to the interaction between the tip apex atom and the surface atom nearest to it, the electron-density profile forms a bridge structure in the intervening vacuum region.

In the present cases, the conventional potential barrier height, which is the concept averaged over the atomic scale variation, no longer has any meaning since the effective potential depends strongly on the positions of the tip on an atomic scale. To see the formation mechanism of the bridge structure between the tip and surface, we show the calculated results of the effective potential as well as the microscopic current distribution. Figure 8 shows contour maps of the effective potential and the current-density distribution for $d=14.0a_B$ (left) and $10.0a_B$ (right) at a bias voltage of $V_S=+2.0$ V. For the contour plots of the effective potential, the potential regions higher than the Fermi level of the tip are shown. These regions correspond to the potential barrier for tunneling electrons. The current density is represented at various spatial points by an arrow whose length is proportional to the current value, and whose direction is parallel to the current. It is seen that the opening of a hole in the potential barrier occurs in the vicinity of the tip apex atom in the case of $14.0a_B$ separation due to the proximity effect of the tip. As mentioned above, the conventional average potential barrier in the lateral direction is no longer physically relevant. In this situation, a small number of electrons is emitted ballistically through a narrow channel of the hole. However, due to the uncertain principle of quantum mechanics, these electrons still feel an effective potential barrier when they pass through such a narrow hole.[2] Correspondingly, the transmission of the electron is reduced even in the presence of the hole. This reflects a small deformation of the electron-density profile, not forming a bridge structure at this separation. With a decrease of the separation, the potential barrier reduces significantly, and correspondingly the opening of this potential barrier becomes wide. At the separation of $10.0a_B$, we can see that only a very small

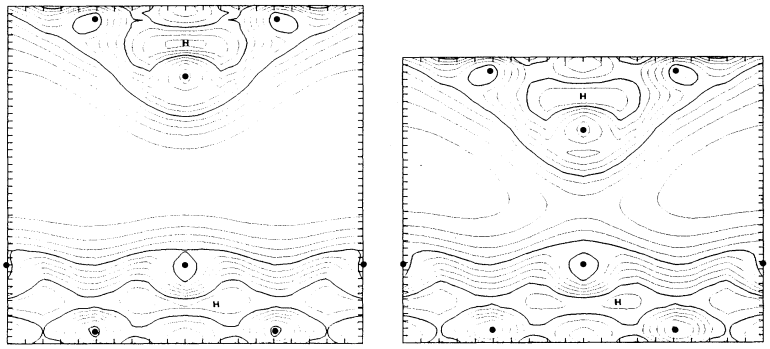

FIG. 7. Electron-density distribution for the tip-surface separation of $d=14.0a_B$ (left) and $10.0a_B$ (right). The applied bias is $V_S=+2.0$ V for both cases. The contour spacing is the same as in Fig. 3.

potential barrier remains far from the tip apex atom, which develops the channels of ballistic electron emission, increases its transmission, and induces the formation of a bridge structure of the electron-density profile between the tip and surface. As will be shown below, the bridge structure of the electron-density profile is also formed with the increase of the applied bias voltage.

As for the current-density distribution, it is well collimated in the vicinity of the tip apex, reflecting the structural feature of the potential barrier. This behavior is different from that of the planar junction, in which the current distribution in the vacuum region is almost uniform. Figure 9 shows how this collimated current density collapses and spreads over in the surface. The top view represents the current density on the $z=0$ plane, in the middle of the vacuum region. The middle view is on the plane of the top surface layer. It is seen that the collimated current density spreads out as a whole. The hollow formed at the center of the collimated current density is due to the collision and scattering with the nearest atom in the top layer of the surface. The bottom view is on the plane on the atoms in the second layer. The collimated structure of the current density disappears completely. The hollows are made due to the scattering with the atoms in the second layer.

V. THEORY OF ATOM MANIPULATION BY STM

Recently STM has been used as a tool for manipulating surface atoms on a nanometer scale. This technology affords possibilities to design artificial materials on an atomic scale, and opened a promising era for STM application. However, the basic mechanisms of atom manipulation are not fully understood. They are related to various surface-atomic processes. The field evaporation due to the strong electric field was first considered to play a dominant role,[7] but the electric field required for atom manipulation by STM has been reported to be much lower than that needed for the field evaporation.[10] Because of the close proximity of the tip and surface, the process is believed to depend strongly on direct chemical interaction in addition to electric field and current. In order to obtain theoretical clues for these problems, we have calculated the electronic states of the tip and surface for several applied bias voltages, changing the position of a single atom located just below the tip atom from the initial atomic configuration toward the direction of the tip. Then the force acting on the removed atom has been calculated in the adiabatic limit, and potential curves obtained by the integration of the force. For simplicity the process that the tip atom is removed is not considered here.

Figure 10 shows the potential curves of the removed atom for various displacements s measured from the original position. The tip atom is fixed at $d=14.0a_B$ apart from the surface. In the zero-bias case, there are two equilibrium positions for the atom considered. One position is located near the surface and the other near the tip atom, approximately $s=9.0a_B$. It is seen that the activation barrier from the surface to the tip is approximately

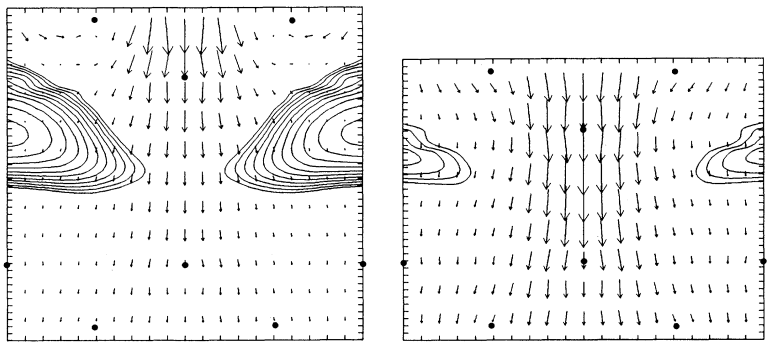

FIG. 8. Effective potential and current-density distribution for the tip-surface separations $d=14.0a_B$ (left) and $10.0a_B$ (right) at a surface bias voltage of $V_S=+2.0$ V. Potential regions higher than the Fermi level of the tip are shown in units of 0.1 eV. The atomic positions are indicated by ●.

0.80 eV, which is larger than the activation barrier 0.52 eV from the tip to the surface. The difference comes from the effect of the shape of the tip. In this case the position near the surface is more stable and thus the atom is not removed in the zero-bias case. As a larger positive applied bias voltage is imposed on the surface, the force acting on the atom increases in the direction of the tip, and correspondingly the activation barrier from the surface to the tip decreases significantly.[33] The activation barrier from the surface to the tip disappears beyond the bias voltage of approximately $V_S = +5.0$ V. For higher applied bias, e.g., $V_S = +8.0$ V, the equilibrium position exists near the tip only. In that case, the atom is removed from the surface and is stabilized near the tip apex atom. Note that even if a small activation barrier remains, the atom can be removed, surmounting it by thermal motion.

In Fig. 11, we show the contour maps of electron-density profiles for the case of no displacement at the surface bias voltage of $V_S = 0$, $+5.0$, and $+8.0$ V, respectively. As the applied bias increases, a remarkable electron distribution is induced in the vicinity of the tip apex atom. It swells from the tip apex toward the vacuum gap due to the negative potential on the tip. Then there appears a region of the electron accumulation just outside the tip apex. Since the region is located near the atom of the top surface just below the tip apex, a significant attractive force is induced toward the accumulated electron clouds. The increase of the attractive force becomes enhanced when a bridge structure is formed between the tip apex and the top surface atom in the vacuum region. One could imagine that the electron cloud induced by the electric field acts as if the chameleon's tongue pulls out the surface atom. This chemical interaction plays an important role for the removal of the specific atom from the surface.

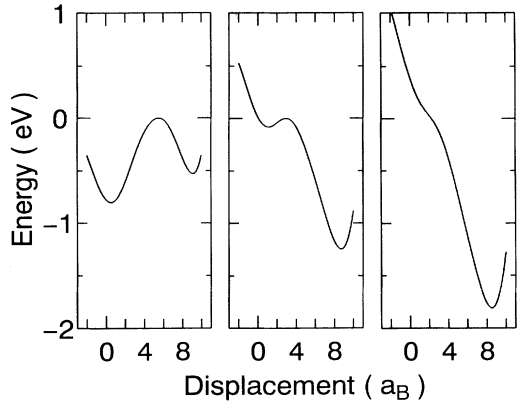

FIG. 10. Adiabatic potential-energy curves of the removed atom at the surface bias voltages of $V_S = 0$ V (left), $+5.0$ V (center), and $+8.0$ V (right), respectively. The displacement is measured from the original atomic position, and the origin of the energy is arbitrary.

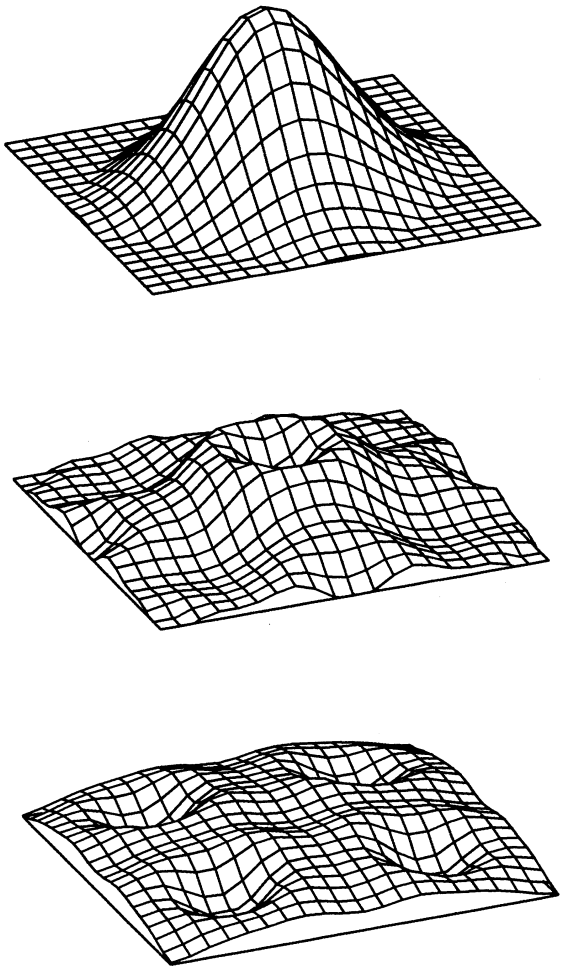

FIG. 9. Collapse of the current density on the plane of $z = 0$ (top), in the top layer of the surface (middle) and in the second layer (bottom). The tip-surface separation is $d = 14.0 a_B$.

Figure 12 shows electron-density profiles for the case of the displacement of $s = 4.0 a_B$, where the removed atom is located in the middle of the tip atom and the surface. At this displacement, accumulation of the electron cloud exists between the extracted atom and the tip apex and also between the extracted atom and other surface atoms. Thus the attractive forces are exerted both from the tip and from the surface, which seem to be of the same order, though the latter force is slightly stronger in the zero-bias case and the former force is stronger in the case of $V_S = +8.0$ V. The bias $V_S + 5.0$ V is the marginal case, where the electron cloud of the removed atom is divided into two, one part attracted from the tip and the other attracted from the surface. This corresponds to the situation in which the activation barrier disappears. Figure 13 shows the electron-density profiles for the displacement of $s = 8.0 a_B$, where the extracted atom is located near the minimum of the potential curves close to the tip. In this case the attractive force toward the tip exceeds that toward the surface. It is seen that chemical bonding is formed between the tip apex and the removed atom, which is extracted completely from the surface.

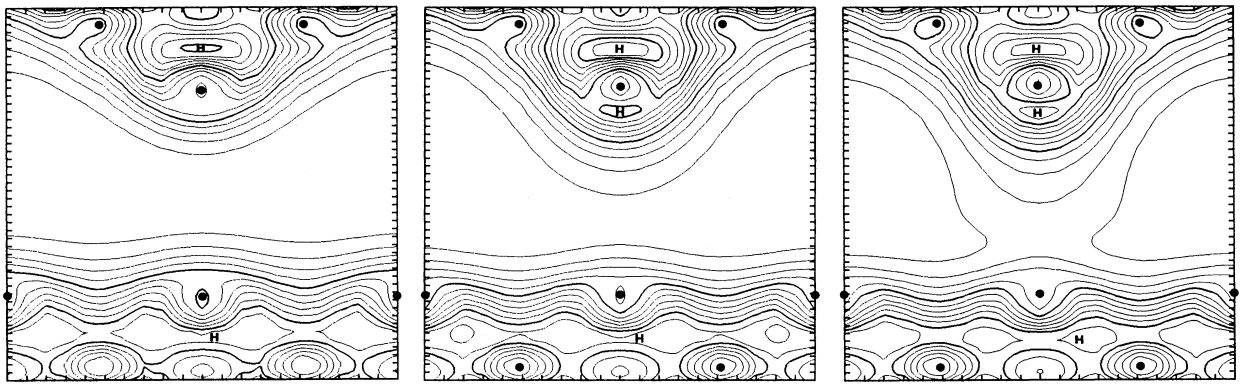

FIG. 11. Electron-density profiles in the (110) plane at the surface bias voltages of $V_S=0$ V (left), $+5.0$ V (center), and $+8.0$ V (right) in the case of no displacement. The contour spacing is the same as in Fig. 3.

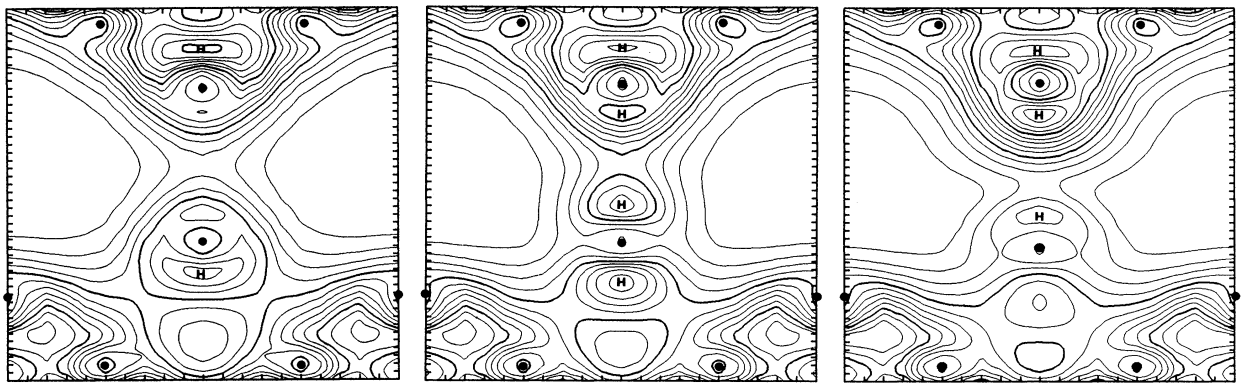

FIG. 12. Electron-density profiles for the displacement of $4.0a_B$ from the original position at the surface bias voltages of $V_S=0$ V (left), $+5.0$ V (center), and $+8.0$ V (right).

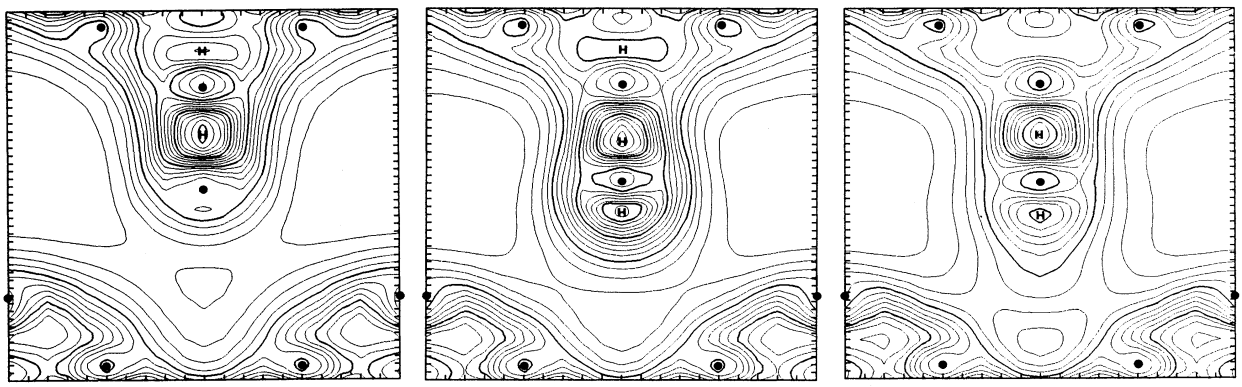

FIG. 13. Electron-density profiles for the displacement of $8.0a_B$ from the original position at the surface bias voltages of $V_S=0$ V (left), $+5.0$ V (center), and $+8.0$ V (right).

VI. SUMMARY AND CONCLUDING REMARKS

We have developed a microscopic theory of nanometer-scale junction under strong field and current based on first-principles calculations. This method goes beyond perturbation theory and enables us to treat various phenomena occurring on the surface under strong electric field and current. The main point of our theoretical approach is as follows: we have treated the junction including both the tip and the surface-atomic structure as a whole and obtained its self-consistent electronic structure. Instead of solving the periodic slab models or cluster models, scattering waves have been used to represent the electronic state for the system in which the electric current is flowing. The coupled-channel equation is solved numerically in the direction normal to the surface, and accurate tails of the wave functions are obtained in the vacuum region without any difficulties of the divergence.

This method has been applied to the Na/vacuum/Na junction system. First the planar junction system has been treated. We have shown that the potential barrier height and the electric current depend strongly on the separation of the surfaces. In the contact region in which the potential barrier disappears, the electron density is deformed significantly due to the strong interaction between the two surfaces.

Then the present method has been extended to the tip-surface system to mimic the STM situation. We have shown that the microscopic shape of the tunnel barrier is dramatically changed near the contact region depending on the tip-surface distance and the bias voltage. With the decrease of the separation, the potential hole becomes wider, develops the channels of ballistic electron emission, and induces the formation of bridge structure of the electron-density profile between the tip and the surface. As for the electron flow, it is collimated in a small region near the tip and then spreads over in the surface.

This method has been used to explore the basic mechanism of atom manipulation by the tip. When a large negative bias is imposed on the tip, the electron cloud swells toward the vacuum and accumulates just outside the tip apex atom. Then the surface top atom is remarkably attracted by the accumulation of the electron density, which causes the extraction of the atom. This effect becomes much enhanced when the electron-density profile forms a bridge structure between the tip apex atom and the top surface atom. This explains the extremely localized nature of the process found in the experiments.

ACKNOWLEDGMENTS

We would like to express thanks to Dr. K. Kuroki and Dr. K. Mitsutake for a number of valuable and stimulating discussions. We are grateful to Professor H. Aoki, Dr. T. Nakayama, Dr. K. Kobayashi, Dr. H. Uchida, and Dr. A. Kobayashi for useful suggestions. The numerical calculations were performed at the Computer Center of the University of Tokyo. This work was partially supported by a Grant-in-Aid from the Ministry of Education, Science and Culture of Japan.

*Present address: Fundamental Research Laboratories, NEC Corporation, 34 Miyukigaoka, Tsukuba, Ibaraki 305, Japan.

[1]E. W. Müller, Phys. Rev. **102**, 618 (1956).
[2]E. Gomer, J. Chem. Phys. **31**, 341 (1959).
[3]H. J. Kreuzer and K. Nath, Surf. Sci. **183**, 591 (1987).
[4]T. T. Tsong, Phys. Rev. B **44**, 13 703 (1991).
[5]B. Binnig and H. Rohrer, IBM J. Res. Dev. **30**, 355 (1986); Rev. Mod. Phys. **59**, 615 (1987).
[6]D. M. Eigler, C. P. Lutz, and W. E. Rudge, Nature (London) **352**, 600 (1991).
[7]H. J. Mamin, P. H. Guethner, and D. Rugar, Phys. Rev. Lett. **65**, 2418 (1990).
[8]I. W. Lyo and P. Avouris, J. Chem. Phys. **93**, 4479 (1990); Science **253**, 173 (1991).
[9]H. Uchida, D. Huang, F. Grey, and M. Aono, Phys. Rev. Lett. **70**, 2040 (1993).
[10]A. Kobayashi, F. Grey, R. S. Williams, and M. Aono, Science **259**, 1724 (1993).
[11]J. Tersoff and D. R. Hamann, Phys. Rev. Lett. **50**, 1998 (1983); Phys. Rev. B **31**, 805 (1985).
[12]M. Tsukada and N. Shima, J. Phys. Soc. Jpn. **56**, 2875 (1987); M. Tsukada, K. Kobayashi, N. Isshiki, and H. Kageshima, Surf. Sci. Rep. **13**, 265 (1991).
[13]J. G. Simmons, J. Appl. Phys. **34**, 1973 (1963).
[14]R. Haydock and D. R. Kingham, Surf. Sci. **103**, 239 (1981).
[15]J. A. Appelbaum and D. R. Hamann, Phys. Rev. B **6**, 2166 (1972).
[16]A. J. Benett and C. B. Duke, Phys. Rev. **160**, 541 (1967); **162**, 578 (1967).
[17]J. Ferrante and J. R. Smith, Phys. Rev. B **19**, 3911 (1979); **31**, 3427 (1985).
[18]L. Orosz and E. Balázs, Surf. Sci. **177**, 444 (1986).
[19]A. McCann and J. S. Brown, Surf. Sci. **194**, 44 (1988).
[20]N. D. Lang, A. Yacoby, and Y. Imry, Phys. Rev. Lett. **63**, 1499 (1989).
[21]N. D. Lang, Phys. Rev. B **45**, 13 599 (1992); **49**, 2067 (1994).
[22]S. Ciraci, A. Baratoff, and I. P. Batra, Phys. Rev. B **41**, 2763 (1990); **42**, 7618 (1990).
[23]K. Hirose and M. Tsukada, Phys. Rev. Lett. **73**, 150 (1994).
[24]J. P. Vigneron and Ph. Lambin, J. Phys. A **13**, 1135 (1980); H. Q. Nguyen, P. H. Cutler, T. E. Feuchtwang, N. Miskovsky, and A. A. Lucas, Surf. Sci. **160**, 331 (1985).
[25]R. M. Nieminen, J. Phys. F **7**, 375 (1977).
[26]N. W. Ashcroft, Phys. Lett. **23**, 48 (1966).
[27]G. Vignale and M. Rasolt, Phys. Rev. Lett. **59**, 2360 (1987); Phys. Rev. B **37**, 10 685 (1988).
[28]D. M. Ceperley and B. J. Alder, Phys. Rev. Lett. **45**, 566 (1980).
[29]J. Perdew and A. Zunger, Phys. Rev. B **23**, 5048 (1981).
[30]N. D. Lang and W. Kohn, Phys. Rev. B **3**, 1215 (1971).
[31]N. D. Lang, Phys. Rev. B **37**, 10 395 (1988).
[32]U. Landman, W. D. Luedtke, N. A. Burnham, and R. J. Col-

ton, Science **248**, 454 (1990).

[33]There is evidence that a single atom can be extracted from a negatively biased surface in STM (Refs. 9 and 10). These experiments have been performed at a larger tip-surface distance in the field evaporation regime. As for the mechanism proposed for them, see T. T. Tsong, Phys. Rev. B **44**, 13 703 (1991); N. M. Miskovsky, C. M. Wei, and T. T. Tsong, Phys. Rev. Lett. **69**, 2427 (1992).